ACS APPLIED MATERIALS & INTERFACES
Letter
www.acsami.org

Thin-Film Barrier Performance of Zirconium Oxide Using the Low-Temperature Atomic Layer Deposition Method

Yu Duan,* Fengbo Sun, Yongqiang Yang, Ping Chen, Dan Yang, Yahui Duan, and Xiao Wang

[†]State Key Laboratory on Integrated Optoelectronics, College of Electronic Science and Engineering, Jilin University, Jilin 130012, China

[‡]College of Science, Changchun University of Science and Technology, Jilin 130022, China

ABSTRACT: In this study, ZrO_2 films deposited by the atomic layer deposition method, as the encapsulation layer for organic electronics devices, were characterized. Both the effects of tetrakis (dimethylamido) zirconium(IV) growth temperature and oxidants, such as water (H_2O) and ozone (O_3), were investigated. The X-ray diffraction analysis shows the amorphous characteristic of the 80-nm-thick films grown at 80 °C, the crystallinity of the films was much lower than those grown at 140 and 200 °C. The scanning electron microscopy analyses showed that the surface morphology strongly depended on the crystallinity of the film. The water vapor transmission rate of the 80 nm thick ZrO_2 films can be reduced from 3.74×10^{-3} g/(m^2 day) (80 °C−H_2O as the oxidant) to 6.09×10^{-4} g/(m^2 day) (80 °C−O_3 as the oxidant) under the controlled environment of 20 °C and a relative humidity of 60%. Moreover, the organic light-emitting diodes integrated with 80 °C−O_3-derived ZrO_2 films were undamaged, and their luminance decay time changed considerably. This was attributed to the better barrier property of the low-temperature ZrO_2 film to the amorphous microscopic bulk and almost homogeneous microscopic surface.

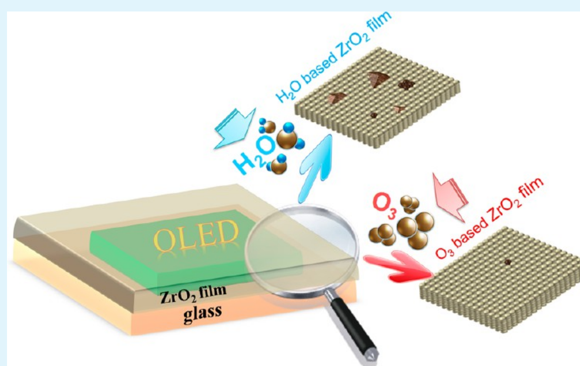

KEYWORDS: *zirconium oxide, thin-film encapsulation, ozone oxidant, atomic layer deposition, crystalline state, water vapor transmission rate*

1. INTRODUCTION

Organic light-emitting diodes (OLEDs) have been a major area of research in organic semiconducting materials and devices.[1] OLEDs have many advantages such as high brightness, high contrast ratio, low cost, ultrathin, and more adaptability for flexible substrates.[2−4] Because of the high sensitivity of organic materials, OLEDs and organic photovoltaic devices require encapsulation of materials to protect them from oxidative species such as water and oxygen.[5−7] When the OLEDs are operated at ambient atmosphere, the formation of dark spots leads to complete device degradation within a few hours.[8] The previous studies indicated that a water vapor transmission rate (WVTR) in the range 1×10^{-6} g/(m^2 day) is needed to reach a minimum OLED lifetime of 10 000 h.[9] The thin-film encapsulation (TFE) has been considered indispensable for future flexible electronics.

The atomic layer deposition (ALD), a promising method for highly uniform thin-film coatings, comprises a series of self-limiting and surface-saturated reactions to form thin conformal films at a controllable rate.[10] Thin films deposited using the ALD method have been increasingly reported for the OLED encapsulation.[11−13] Films prepared by the ALD method are generally smooth for amorphous and single-crystal epitaxial films; however, polycrystalline films are often rough because of the growth of facets on the crystallites.[14] In addition to roughness, polycrystalline films may lack the high gas barrier that has been associated with the grain boundaries of highly crystalline films.[15] The inhibition of crystallite nucleation and retardation of crystallite growth are two general ALD strategies to control the crystallinity-associated surface roughness. The formation of crystallites can be prevented at low-temperature deposition; however, the ALD precursors generate unacceptable levels of impurities at low-temperature deposition.[10,16] Besides low-temperature deposition, the crystallite growth and associated surface roughness can also be inhibited with the periodic introduction of a second metal oxide that produces an amorphous film in between several polycrystalline regions (a nanolaminate structure). Recently, several studies have focused on developing a better moisture-protective film using Al_2O_3 and ZrO_2 nanolaminate films.[17−19] However, the nanolaminate fabrication process is complex. In this study, to achieve the low-temperature deposition of pure and smooth films, we investigated ZrO_2 films deposited by the ALD method using very reactive ozone (O_3) instead of H_2O as the oxidant. The crystalline ZrO_2 films were suppressed; therefore, the water barrier properties improved significantly.

Received: January 15, 2014
Accepted: March 5, 2014
Published: March 5, 2014

© 2014 American Chemical Society

2. EXPERIMENTAL SECTION

The ZrO_2 films were deposited by the ALD method using a LabNano 9100 ALD system (Ensure Nanotech Inc.). The chamber pressure was 3×10^{-2} Pa. Tetrakis(dimethylamide) zirconium(IV) and H_2O or O_3 were used as the precursors of Zr and O, respectively. The warm-wall reactor was operated at the temperatures 80 °C, 140 °C, and 200 °C. High-purity N_2 at a flow rate of 20 standard cubic centimeter per minute (SCCM) was used as the carrier gas for the precursors. A mixture of oxygen (400 SCCM, 99.999%) and catalytic nitrogen (5 SCCM) was used to provide 3.5 wt % O_3 at a concentration of ~50 mg/L. The X-ray photoemission spectroscopy (XPS) was performed using a Scienta ESCA 200 spectrometer in ultrahigh vacuum with a base pressure of 1×10^{-10} mbar. The measurement chamber was equipped with a monochromatic Al KR X-ray source to afford photons with 1486.6 eV. The scanning electron microscopy (SEM) was performed using a field-emission SEM (JSM-6700F, JEOL) operated at an accelerating voltage of 10 kV, and the samples were coated with a thin layer of gold (5 nm) before the analysis. The water contact angles were measured using a Krüss contact angle goniometer (model DSA30), where the sessile drop of 2−3 μL was dispensed using a micro syringe. The phase and crystallinity of the films were determined by the X-ray diffraction (XRD, model D/max 2400). The high-angle XRD data were collected at 0.05° increments and 15 s count times using the films deposited on the silicon (Si) substrates. The Scherrer's method was used to calculate the average height of the crystallites.

3. RESULTS AND DISCUSSION

3.1. X-ray Photoemission Spectroscopy. The chemical bonding structure of ZrO_2 film on Si substrate was examined using XPS. Figure 1a shows two peaks in the ranges 181.3−181.9 eV and 183.7−184.3 eV corresponding to Zr $3d_{5/2}$ and $3d_{3/2}$ features, respectively. In order to show the influence of the temperature of film deposition on the stoichiometry of the ZrO_2 films, we compared the O/Zr atomic percentage ratio for films deposited at various temperatures. The area below the XPS peak is proportional to the amount of the element on the surface, regardless of the chemical state of the element. The XPS sensitivity factor is 1.11 for Zr 3d and 0.66 for O1s.[20] The O/Zr ratio were 2.2 (200 °C−H_2O as the oxidant), 2.5 (80 °C−H_2O as the oxidant), and 2.1 (80 °C−O_3 as the oxidant), all of which were higher than the stoichiometric values (≈ 2.0) expected for ZrO_2. This observation may be attributed to the presence of hydroxyl species such as Zr−O−OH, allows more atomic oxygen to be incorporated into the film. This phenomenon commonly occurs during lower temperature ALD. Therefore, at 80 °C and using H_2O as the oxidant, the O/Zr ratio of the film was 2.5, indicating that this film contains excess hydroxide. Both ZrO_2 films that used H_2O as oxidant showed a shift of the $Zr3d_{5/2}$ peak into higher binding energies from 181.3 eV (80 °C) to 181.9 eV (200 °C), because the $Zr3d_{5/2}$ component position was in agreement with the formation of Zr(IV) oxide. We attribute this shift toward high BE to the full oxidation of ZrO_2 films deposited at higher temperatures.[21] When O_3 was used as the oxidant, the $Zr3d_{5/2}$ peak shifted to ~0.4 eV toward high BE from 181.3 eV (80 °C−H_2O as the oxidant) to 181.7 eV for (80 °C−O_3 as the oxidant). As the O/Zr ratio was near the stoichiometric value, the film deposited at 80 °C using O_3 as the oxidant may include

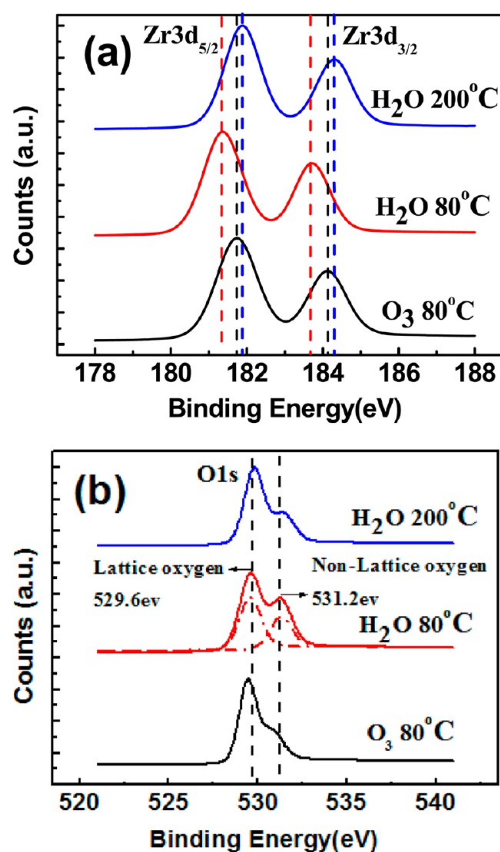

Figure 1. High-resolution XPS spectra of (a) Zr 3d and (b) O1S of ZrO_2 films deposited by the ALD method at 80 and 200 °C using H_2O as the oxidant and at 80 °C using O_3 as the oxidant.

less hydroxide. Figure 1(b) shows the O1s XPS spectra of the ZrO_2 films. The O1s peak was of the sum of two contributions. The main O1s peak component at 529.9 eV was assigned to the lattice oxygen in ZrO_2, whereas the second peak at 531.2 eV was assigned to the surface hydroxide and adsorbed H_2O.[22,23] The ZrO_2 film deposited at 80 °C using O_3 as the oxidant exhibited the lowest content of nonlattice oxygen atoms, where the O_3 film plays an important role as active oxidant to support a complete reaction. Because O_3 molecules have a lower dipole momentum compared to H_2O molecules, which has a high surface affinity, low temperatures generate excess residual hydroxyl groups. Therefore, ZrO_2 film deposited at a low temperature using O_3 as the oxidant was homogeneous and stoichiometric with a relatively low level of impurities.

3.2. X-ray Diffraction Analysis. The XRD spectra of 80 nm thick as-ALD deposit ZrO_2 films at several deposition temperatures are shown in Figure 2. Similar results were observed for both the H_2O- and O_3-based ZrO_2 films as shown in panels a and b in Figure 2. At a deposition temperature of 80 °C, a relative lower peak was observed in the XRD pattern compared with the two higher temperatures, which indicated that this film was mostly amorphous. The formation of crystalline ZrO_2 increased with increasing deposition temperature (80, 140, and 200 °C), and noticeably, a preferred orientation in the (200) direction was observed. The intensity of the peaks increased with increasing deposition temperature. This is in agreement with the results of the earlier reports on ZrO_2 films, where both monoclinic and cubic phases exsited.[24] These films showed some crystallinity. Interestingly, at the same deposition temperature, the average heights of the

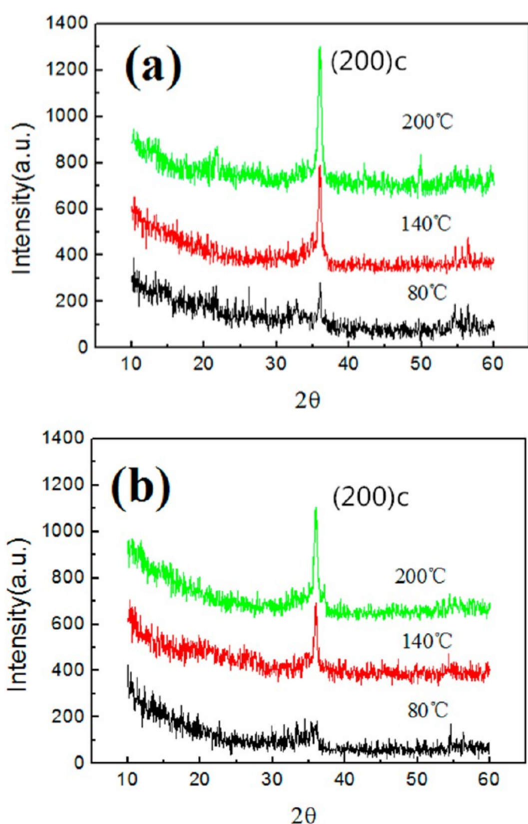

Figure 2. Portion of the XRD pattern: (a) H_2O- and (b) O_3-based ZrO_2 films deposited at different temperatures.

crystallites corresponding to O_3-based ZrO_2 films were lower than the H_2O-based ZrO_2 films as listed in Table 1. This is probably because O_3 has a higher chemical reactivity compared to H_2O; therefore, it hinders the growth of the crystallites and does not contribute to the nucleation events.[16] These results indicated that O_3, as the oxidant, showed better inhibition of crystallization on the surface of ZrO_2 films.

Table 1. Average Height of the Crystallites Was Determined by the XRD for H_2O- and O_3-Based ZrO_2 Films Deposited at Different Temperatures

deposition temperature (°C)	height of H_2O-based ZrO_2 film (nm)	height of O_3-based ZrO_2 film (nm)
80	8.4 ± 0.1	3.8 ± 0.1
140	14.7 ± 0.2	10.7 ± 0.1
200	21.0 ± 0.2	15.2 ± 0.2

3.3. SEM and Water Contact Angles. The morphological properties of the ZrO_2 films deposited directly on the clean Si substrates by the ALD method were studied by the SEM. The 80 °C−H_2O based ZrO_2 film showed slight crystalline grain characteristics (Figure 3), and the crystallinity of the H_2O-based ZrO_2 film deposited on the Si substrate increased with increasing deposition temperature as shown in Figure 3a−c. However, the O_3-based ZrO_2 film at a low temperature of 80 °C (Figure 3d) exhibited an almost homogeneous surface (Figure 3d). As shown in Figure 3d−f, the crystallinity of the O_3-based ZrO_2 films increased with increasing deposition temperature. However, it exhibited lower crystallinity and significant smoothness, which were consistent with the XRD analysis. To further investigate the macroscopic surface behaviors of ZrO_2 film deposited by the ALD method, we analyzed the water contact angles. As shown in the inset of Figure 3a−f, at the same deposition temperature, all O_3-based films showed the relative larger contact angles than its corresponding H_2O-based one, and the improving hydrophobic properties. This phenomenon can be explained because water easily spread across the film with hydroxyl species on surface. Especially, in the case of ZrO_2 with H_2O as the oxidant, the hydroxyls generated because the H_2O reaction with the TMA groups did not complete. Furthermore, hydroxyl groups such as Zr−O−OH strengthened the formation of the crystalline state. However, O_3 has a higher chemical reactivity to TMA, and less residual hydroxyls were accumulated on the surface than the reaction in H_2O.[16]

3.4. Measurement of Water Vapor Transmission Rate. To evaluate the permeability of the ZrO_2 film deposited by the ALD method as water diffusion barrier, the WVTR measurements were performed by the calcium (Ca) corrosion test method, which is used to monitor the resistivity changes resulting in an ohmic behavior. The Ca layer with the thickness and area of 200 nm and 1 × 1 cm^2, respectively, was deposited on a clean glass lined with 100 nm patterned-Al electrodes. The electrical measurements were performed using two electrodes connected by a source measure unit probe to an Agilent 2920 source meter. The change in conductance as a function of time, and the slope dG/dt is used to calculate effective WVTR values according to the following equation[25]

$$\text{WVTR (g/(m}^2\text{ day))} = -n\delta_{\text{Ca}}\rho_{\text{Ca}}\frac{d}{dt}\left(\frac{1}{R}\right)\frac{M(\text{H}_2\text{O})}{M(\text{Ca})}\frac{\text{Ca Area}}{\text{Window Area}} \quad (1)$$

where n is the molar equivalent of the degradation reaction which is assumed to be $n = 2$ based on the chemical reaction of Ca with water [$Ca + 2H_2O$ ($n = 2$) → $Ca(OH)_2 + H_2$]. In eq 1, δ_{Ca} and ρ_{Ca} are the Ca resistivity (3.4×10^{-8} Ω m) and density (1.55 g/cm^3), $M(H_2O)$ and $M(Ca)$ are the molar masses of water (18 amu) and of Ca (40 amu), respectively. The ratio of the area of the Ca sensor to the area of the window for water permeation and the ratio of the length is 1 because of the geometry of the experimental setup. Figure 4 shows the changes in the WVTR with the temperature and oxide precursors. The O_3-based ZrO_2 films exhibited a more stable trend for the conductivity vs operational time. The WVTRs of 80 °C−O_3-based, 80 °C−H_2O-based, 140 °C−O_3-based, and 140 °C−H_2O-based ZrO_2 films were 6.09×10^{-4}, 3.74×10^{-3}, 1.22×10^{-2}, and 8.27×10^{-2} g/(m^2 day), respectively. This result showed that the O_3-based ZrO_2 films deposited at 80 °C exhibited a better water-barrier performance. As shown in panels a and c in Figure 5, the as-deposited Ca films had an intact and opaque area. These Ca films were stored under a controlled environment of 20 °C and relative humidity (RH) of 60%, and after 50 h, a part of the Ca layer became more transparent with time as shown in Figure 5b. This indicated that the film had a low barrier performance in air, which can penetrate inside the TFE, then reacted with the Ca film. However, as shown in Figure 5d, after 50 h, the film did not show any significant change, indicating the slow degradation of the Ca film. This demonstrated that the O_3-based ZrO_2 film had a higher water-barrier performance. In fact, the author should underline that both H_2O and O_2 in air were responsible for the aforementioned Ca film degradation. However, because the climatic chamber can only setup a controlled moisture and

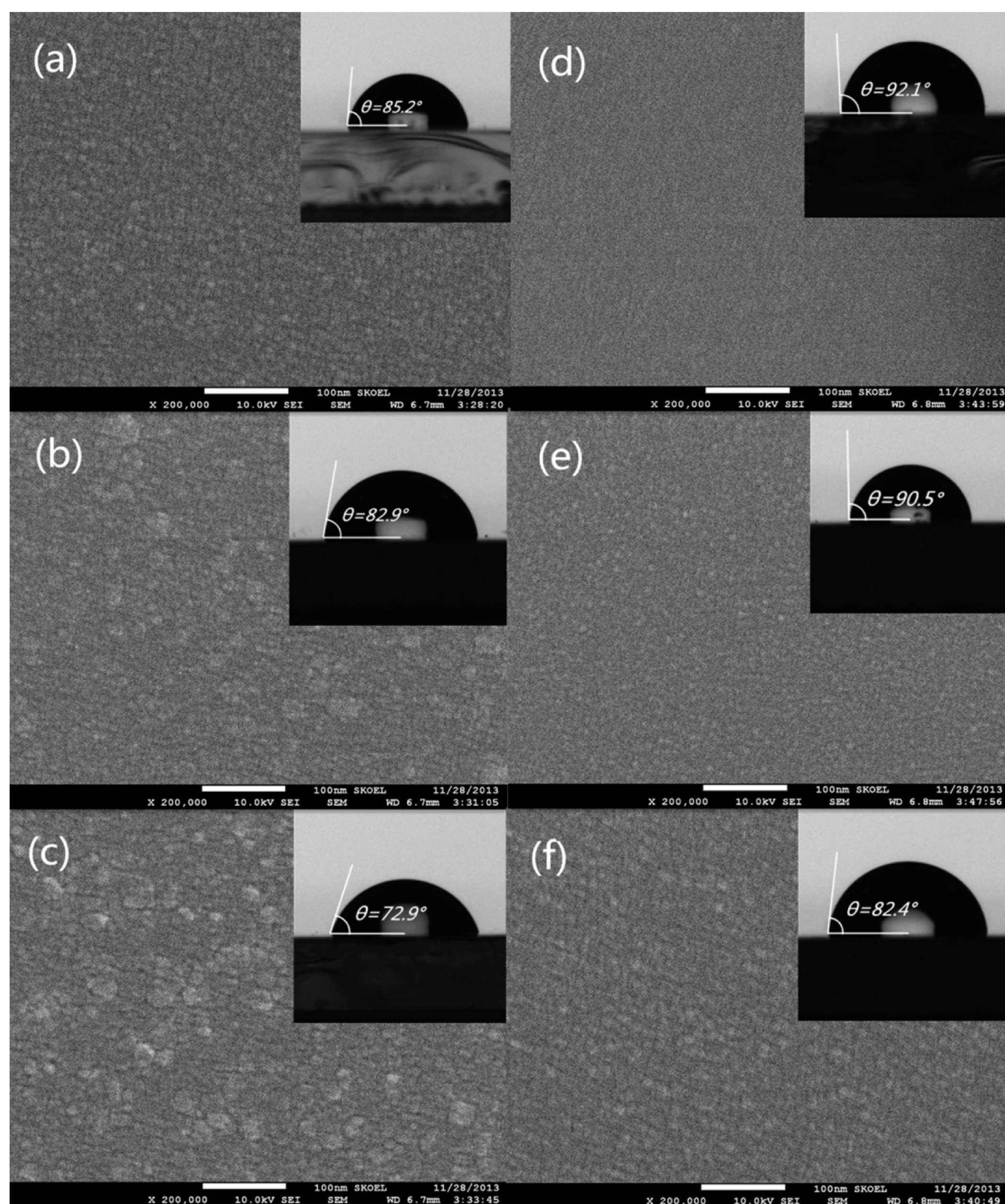

Figure 3. SEM images and water contact angles (inset) of the ALD films deposited on the Si substrate: (a) 80 °C−H_2O-based ZrO_2 film; (b) 140 °C−H_2O-based ZrO_2 film; (c) 200 °C−H_2O-based ZrO_2 film; and (d−f) 80, 140, and 200 °C−O_3-based ZrO_2 films, respectively.

temperature conditions, which was helpful for accurate determination of WVTR, but inappropriate for oxygen transmission rate (OTR). The quantitative OTR analysis was not included in this study, regarding as the contribution of the Ca reaction with O_2 may lower than 5%.[25]

3.5. ZrO_2 Film Encapsulation for OLEDs. Figure 6 shows the typical plots of the normalized luminance vs operating time for the OLEDs with various encapsulations. Besides TFE, the traditional glass cap encapsulation device, which uses UV-curable epoxy NOA63 (NOA63 from Norland Optics) as adhesive between the glass cap and the substrate, was also used to evaluate the effect of TFE on OLED lifetime. The OLED structures were indium−tin-oxide glass/5-nm-thick MoO_3 layer, 30-nm-thick 4,4′,4″-tris (*N*-3(3-methylphenyl)-*N*-phenylamino)triphenyl amine (*m*-MTDATA) as the hole-injection layer; a 20-nm-thick *N*,*N*′-biphenyl-*N*,*N*′-bis(1-naphenyl)-[1,1′-biphenyl]-4,4′-diamine (NPB) as the hole-transport layer; a 50-nm-thick *tris*(8-hydroxyquinoline) aluminum (Alq_3) as the light-emitting and electron-transport layers; and a 1-nm-thick LiF capping with a 120-nm-thick Al cathode. The electrical and emission characteristics of the devices were measured simultaneously using an Agilent 2920 source meter and a Minolta luminance meter LS-110 in air at room temperature. The dependence of the luminance vs operating time was measured at a constant dc voltage. The lifetimes of the OLEDs were measured from an initial luminance of approximately L_0 = 1000 cd/m^2. We studied the devices using 80 °C ALD TFE, because the OLEDs degradation at the temperature >140 °C is very fast, severely damaging during the ALD. As shown in the inset of Figure 6, only a slight difference in the $L-V$ behavior between the nonencapsulated and encapsulated devices was observed. This result indicated that

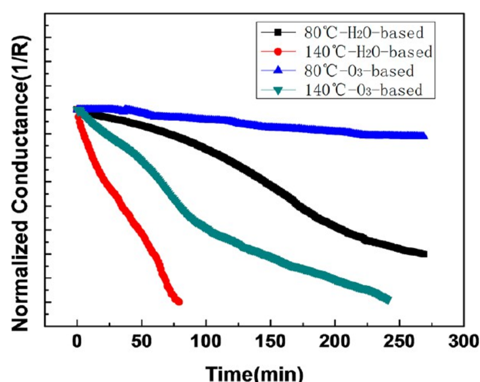

Figure 4. Dependence of the normalized conductance vs time of the Ca corrosion tests at 80 and 140 °C for H_2O- and O_3-based ZrO_2 films deposited at the controlled environment of 20 °C and 60% RH.

the deposition temperature, 80 °C, did not deteriorate the devices. As shown in Figure 6, the bare device in controlled ambient air degraded faster than the OLEDs with TFE, indicating that the degradation caused by O_2 and H_2O permeating inside devices. The OLEDs with O_3-based TFE had a lifetime of 39 h with an elapsed time of the instantaneous luminance decay to 70% of its initial value, and it was comparable with devices encapsulated with a glass cap and approximately 6- and 2.3-folds longer than the bare device and H_2O-based TFE, respectively.

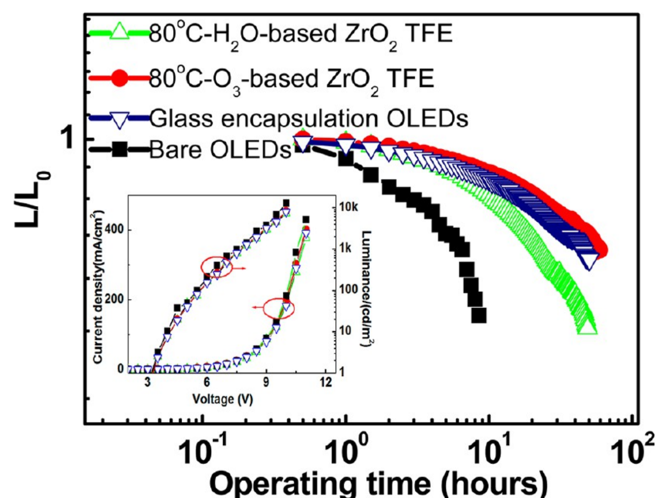

Figure 6. Normalized luminance decay as a function of continuous operation time for OLEDs with or without TFE, measured under 20 °C, 60% RH. The inset shows luminance and current vs operational voltage characteristics of bare OLED and the encapsulated OLEDs with 80 °C−H_2O-, 80 °C−O_3-based ZrO_2 films and glass cap.

4. CONCLUSION

In summary, we successfully synthesized amorphous and homogeneous ZrO_2 thin films for the OLEDs TFE using O_3 as the oxidant. Based on the detailed chemical and physical investigations, the 80 nm thick ZrO_2 films deposited at the low temperature using O_3 as the oxidant exhibited a lower surface crystallinity compared with those films using H_2O as oxidant or grown under higher temperature. In this approach, fine amorphous microscopic bulk and almost homogeneous microscopic surface behaviors improved the gas barrier properties. The WVTR of 80 nm thick ZrO_2 films was reduced from 3.74×10^{-3} g/(m^2 day) (80 °C−H_2O-based) to 6.09×10^{-4} g/(m^2 day) (80 °C−O_3-based) and exhibited a longer continuous operation lifetime of 2.3 folds than the device using H_2O-based ZrO_2 TFE under the identical conditions. Further studies will focus on using more reactive oxidants to evaluate the hard metal oxide coating by the ALD method to investigate their functional properties for the dielectric and optical applications.

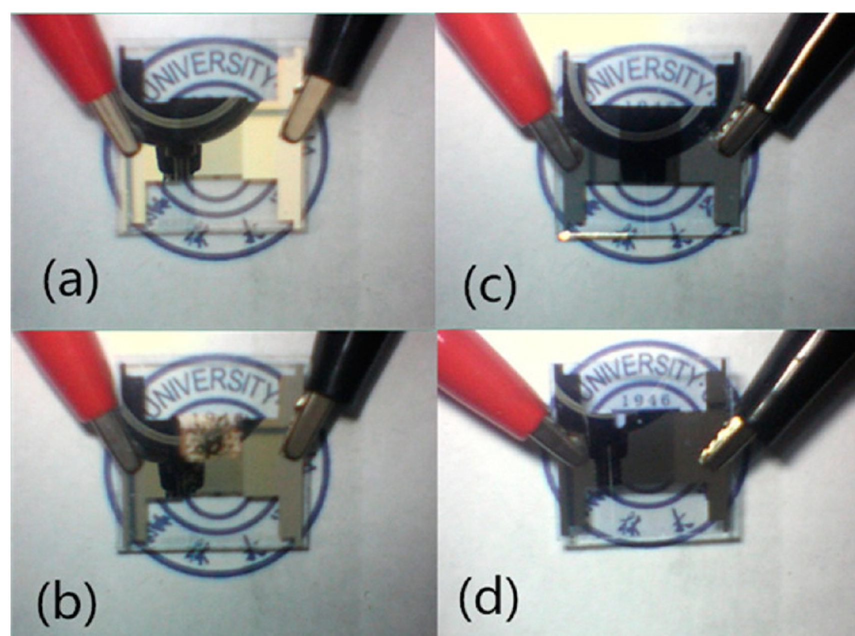

Figure 5. Optical images of the Ca corrosion test device at the controlled environment, 20 °C and 60% RH, encapsulated with (a) and (b) 80-nm-thick 80 °C−H_2O-based ZrO_2 TFE after 0 and 50 h tests, respectively, (c) and (d) 80 nm thick 80 °C−O_3-based ZrO_2 TFE after 0 and 50 h tests, respectively.

AUTHOR INFORMATION

Corresponding Author

*E-mail: duanyu@jlu.edu.cn.

Notes

The authors declare no competing financial interest.

ACKNOWLEDGMENTS

This study was supported by the National High Technology Research and Development Program of China (Grant 2011AA03A110), Ministry of Science and Technology of China (Grant 2010CB327701 and 2013CB834802), National Natural Science Foundation of China (Grants 61275024, 61274002, 61275033, 61177025, 6137706, and 41001302), Scientific and Technological Developing Scheme of Jilin Province (Grant 201101034), Research Fund for the Doctoral Program of Higher Education (Grant 20070183088), and Opened Fund of the State Key Laboratory on Integrated Optoelectronics No. IOSKL2012KF01.

REFERENCES

(1) Reineke, S.; Lindner, F.; Schwartz, G.; Seidler, N.; Walzer, K.; Lüssem, B.; Leo, K. White Organic Light-Emitting Diodes with Fluorescent Tube Efficiency. *Nature* **2009**, *459*, 234−238.

(2) Meyer, J.; Schneidenbach, D.; Winkler, T.; Hamwi, S.; Weimann, T.; Hinze, P.; Ammermann, S.; Johannes, H.-H.; Riedl, T.; Kowalsky, W. Reliable Thin Film Encapsulation for Organic Light Emitting Diodes Grown by Low-Temperature Atomic Layer Deposition. *Appl. Phys. Lett.* **2009**, *94*, 233305−233305.

(3) Duan, Y.; Mazzeo, M.; Cheng, G.; Mariano, F.; Gigli, G. High-Efficiency Red Phosphorescent Electroluminescence Devices Based on Mixed P/N Host Matrices. *Opt. Lett.* **2010**, *35*, 3174−3176.

(4) Zhu, Y. C.; Zhou, L.; Li, H. Y.; Xu, Q. L.; Teng, M. Y.; Zheng, Y. X.; Zuo, J. L.; Zhang, H. J.; You, X. Z. Highly Efficient Green and Blue-Green Phosphorescent OLEDs Based on Iridium Complexes with the Tetraphenylimidodiphosphinate Ligand. *Adv. Mater.* **2011**, *23*, 4041−4046.

(5) Do, L. M.; Oyamada, M.; Koike, A.; Han, E. M.; Yamamoto, N.; Fujihira, M. Morphological Change in the Degradation of Al Electrode Surfaces of Electroluminescent Devices by Fluorescence Microscopy and AFM. *Thin Solid Films.* **1996**, *273*, 209−213.

(6) Weaver, M. S.; Michalski, L. A.; Rajan, K.; Rothman, M. A.; Silvernail, J. A.; Brown, J. J.; Burrows, P. E.; Graff, G. L.; Gross, M. E.; Zumhoff, M. Organic Light-Emitting Devices with Extended Operating Lifetimes on Plastic Substrates. *Appl. Phys. Lett.* **2002**, *81*, 2929−2931.

(7) Wuu, D. S.; Chen, T. N.; Lay, E.; Liu, C. H.; Chang, C. H.; Wei, H. F.; Wei, H. F.; Jiang, L. Y.; Lee, H. U.; Chang, Y. Y. Transparent Barrier Coatings on High Temperature Resisting Polymer Substrates for Flexible Electronic Applications. *J. Electrochem. Soc.* **2010**, *157*, C47−C51.

(8) Schaer, M.; Nüesch, F.; Berner, D.; Leo, W.; Zuppiroli, L. Water Vapor and Oxygen Degradation Mechanisms in Organic Light Emitting Diodes. *Adv. Funct. Mater.* **2001**, *11*, 116−121.

(9) Zhou, Z.; Wang, Z.; Yi, Y.; Jiang, S.; Wang, G.; Chen, J. Properties and Micro-Structure of ZrO_2−Al_2O_3 Composites with Three-Layer Structure. *Compos. Part. B-eng.* **2011**, *42*, 1271−1275.

(10) George, S. M. Atomic Layer Deposition: An Overview. *Chem. Rev.* **2009**, *110*, 111−131.

(11) Yun, S. J.; Ko, Y. W.; Lim, J. W. Passivation of Organic Light-Emitting Diodes with Aluminum Oxide Thin Films Grown by Plasma-Enhanced Atomic Layer Deposition. *Appl. Phys. Lett.* **2004**, *85*, 4896−4898.

(12) Ghosh, A. P.; Gerenser, L. J.; Jarman, C. M.; Fornalik, J. E. Thin-Film Encapsulation of Organic Light-Emitting Devices. *Appl. Phys. Lett.* **2005**, *86*, 223503−223505.

(13) Carcia, P. F.; McLean, R. S.; Reilly, M. H.; Groner, M. D.; George, S. M. Ca Test of Al_2O_3 Gas Diffusion Barriers Grown by Atomic Layer Deposition on Polymers. *Appl. Phys. Lett.* **2006**, *89*, 031915−031915.

(14) Gocmez, H.; Fujimori, H.; Tuncer, M.; Gokyer, Z.; Duran, C. The Preparation and Characterization of Al_2O_3/ZrO_2 Nanocrystalline Composite by a Simple Gel Method. *Mater. Sci. Eng., B* **2010**, *173*, 80−83.

(15) Choi, D. W.; Kim, S. J.; Lee, J. H.; Chung, K. B.; Park, J. S. A Study of Thin Film Encapsulation on Polymer Substrate Using Low Temperature Hybrid ZnO/Al_2O_3 Layers Atomic Layer Deposition. *Curr. Appl. Phys.* **2012**, *12*, S19−S23.

(16) Yang, Y. Q.; Duan, Y.; Chen, P.; Sun, F. B.; Duan, Y. H.; Wang, X.; Yang, D. Realization of Thin Film Encapsulation by Atomic Layer Deposition of Al_2O_3 at Low Temperature. *J. Phys. Chem.C* **2013**, *117*, 20308−20312.

(17) Meyer, J.; Schmidt, H.; Kowalsky, W.; Riedl, T.; Kahn, A. The Origin of Low Water Vapor Transmission Rates through Al_2O_3/ZrO_2 Nanolaminate Gas-Diffusion Barriers Grown by Atomic Layer Deposition. *Appl. Phys. Lett.* **2010**, *96*, 243308−243310.

(18) Meyer, J.; Görrn, P.; Bertram, F.; Hamwi, S.; Winkler, T.; Johannes, H. H.; Weimann, T.; Hinze, P.; Riedl, T.; Kowalsky, W. Al_2O_3/ZrO_2 Nanolaminates as Ultrahigh Gas-Diffusion Barriers—A Strategy for Reliable Encapsulation of Organic Electronics. *Adv. Mater.* **2009**, *21*, 1845−1849.

(19) Meyer, J.; Schneidenbach, D.; Winkler, T.; Hamwi, S.; Weimann, T.; Hinze, P.; Ammermann, S.; Johannes, H. H.; Riedl, T.; Kowalsky, W. Reliable thin film encapsulation for organic light emitting diodes grown by low-temperature atomic layer deposition. *Appl. Phys. Lett.* **2009**, *94*, 233305−233307.

(20) Wagner, C. D.; Riggs, W. M.; Davis, L. E.; Moulder, J. F.; Mullenberg, G. E. *Handbook of X-ray Photoelectron Spectroscopy*; Perkin-Elmer Corp: Eden Prairie, MN, 1979.

(21) Kim, S. K.; Lee, S. W.; Hwang, C. S.; Min, Y. S.; Won, J. Y.; Jeong, J. Low Temperature (< 100°C) Deposition of Aluminum Oxide Thin Films by ALD with O3 as Oxidant. *J. Electrochem. Soc.* **2006**, *153*, F69−F76.

(22) Barreca, D.; Battiston, G. A.; Gerbasi, R.; Tondello, E.; Zanella, P. Zirconium Dioxide Thin Films Characterized by XPS. *Surf. Sci. Spectra* **2000**, *7*, 303.

(23) Samanipour, F.; Bayati, M. R.; Golestani-Fard, F.; Zargar, H. R.; Troczynski, T.; Mirhabibi, A. R. An Innovative Technique to Simply Fabricate ZrO_2−HA−TiO_2 Nanostructured Layers. *Colloids Surf., B* **2011**, *86*, 14−20.

(24) Hausmann, D. M.; Gordon, R. G. Surface Morphology and Crystallinity Control in the Atomic Layer Deposition (ALD) of Hafnium and Zirconium Oxide Thin films. *J. Cryst. Growth.* **2003**, *249*, 251−261.

(25) Paetzold, R.; Winnacker, A.; Henseler, D.; Cesari, V.; Heuse, K. Permeation Rate Measurements by Electrical Analysis of Calcium Corrosion. *Rev. Sci. Instrum.* **2003**, *74*, 5147−5150.